Published in final edited form as:
Development. 2008 February ; 135(4): 729–741. doi:10.1242/dev.013276.

Cux2 (*Cutl2*) integrates neural progenitor development with cell-cycle progression during spinal cord neurogenesis

Angelo Iulianella[1], **Madhulika Sharma**[2], **Michael Durnin**[1], **Greg B. Vanden Heuvel**[2], and **Paul A. Trainor**[1,2,*]

[1]Stowers Institute for Medical Research, 1000 E. 50th Street, Kansas City, MO 64110, USA

[2]Department of Anatomy and Cell Biology, University of Kansas Medical Center, Kansas City, KS 66160, USA

Abstract

Neurogenesis requires the coordination of neural progenitor proliferation and differentiation with cell-cycle regulation. However, the mechanisms coordinating these distinct cellular activities are poorly understood. Here we demonstrate for the first time that a Cut-like homeodomain transcription factor family member, *Cux2* (*Cutl2*), regulates cell-cycle progression and development of neural progenitors. *Cux2* loss-of-function mouse mutants exhibit smaller spinal cords with deficits in neural progenitor development as well as in neuroblast and interneuron differentiation. These defects correlate with reduced cell-cycle progression of neural progenitors coupled with diminished Neurod and $p27^{Kip1}$ activity. Conversely, in *Cux2* gain-of-function transgenic mice, the spinal cord is enlarged in association with enhanced neuroblast formation and neuronal differentiation, particularly with respect to interneurons. Furthermore, *Cux2* overexpression induces high levels of Neurod and $p27^{Kip1}$. Mechanistically, we discovered through chromatin immunoprecipitation assays that *Cux2* binds both the *Neurod* and $p27^{Kip1}$ promoters in vivo, indicating that these interactions are direct. Our results therefore show that *Cux2* functions at multiple levels during spinal cord neurogenesis. *Cux2* initially influences cell-cycle progression in neural progenitors but subsequently makes additional inputs through *Neurod* and $p27^{Kip1}$ to regulate neuroblast formation, cell-cycle exit and cell-fate determination. Thus our work defines novel roles for *Cux2* as a transcription factor that integrates cell-cycle progression with neural progenitor development during spinal cord neurogenesis.

Keywords

Cut-like; Cux; Spinal cord; Neurogenesis; Interneurons; Motoneurons; Neurod1; $p27^{Kip1}$; Cell cycle; Mouse

INTRODUCTION

Neurogenesis requires the complex integration of neural progenitor proliferation, cell-cycle exit, migration and differentiation. In the developing nervous system, neural stem cells are present in embryonic day (E) 8.5–9.5 mouse embryos within the neuroepithelium, where they proliferate extensively through symmetric cell divisions. Shortly thereafter, these neural stem cells are referred to as radial glia, reflecting their generation of a neuron followed by a radial glial cell through asymmetric cell division (McConnell, 1995; Temple, 2001). The

*Author for correspondence (pat@stowers-institute.org).

Supplementary material Supplementary material for this article is available at http://dev.biologists.org/cgi/content/full/135/4/729/DC1

coupling of cell-cycle exit to differentiation programs ensures the correct numbers of neuronal subtypes are consistently generated to form functional neural circuits (Kintner, 2002). Of central importance to this process is the decrease in expression of progenitor determinants, the increase in cell-cycle inhibitors and the implementation of cell-fate specification programs (Durand and Raff, 2000; Jessell, 2000). How these processes are coordinated remains the focus of active investigation.

The spinal cord has been used extensively as a model of neuronal differentiation and much is known about the regulatory control of dorsoventral patterning in response to growth factor signaling (Lupo et al., 2006; Poh et al., 2002; Zhuang and Sockanathan, 2006). Graded Sonic hedgehog (Shh) signaling from the ventral neural tube induces the formation of ventral cell types, including ventral interneurons and motoneurons, while Wingless/int-related (Wnt) and Bone morphogenetic protein (BMP) signaling from the dorsal neural tube influences the formation of dorsal interneurons. In addition, Notch signaling may also be important for directing both ventral and dorsal interneuron fate (Mizuguchi et al., 2006; Yang et al., 2006); however, its primary role is to promote neural progenitor maintenance (Androutsellis-Theotokis et al., 2006).

The first neurons to be born in the spinal cord are interneurons, followed by ventral motoneurons (Sechrist and Bronner-Fraser, 1991), and central to the formation of both interneurons and motoneurons is the control of cell-cycle exit in neural progenitor populations by the G1 cyclin inhibitor $p27^{Kip1}$ (Fero et al., 1996; Gui et al., 2007; Kiyokawa et al., 1996; Nakayama et al., 1996). Although it is not clear how the generation of cell type diversity is coupled to cell-cycle withdrawal during neurogenesis, it has been suggested that the length of the cell cycle may impact directly on cell-fate determination (Shen et al., 2006; Wilcock et al., 2007).

The *Cut* gene family comprises a unique group of homeodomain transcription factor proteins containing one or more Cut repeat DNA-binding domains. In *Drosophila* embryos, *Cut* is a Notch signaling target gene required for external sensory organ development of cells already committed to the proneural lineage (Blochlinger et al., 1990; Blochlinger et al., 1991; Bodmer et al., 1987). In vertebrates, two *Cut* homologs *Cux1* (*Cutl1*) and *Cux2* (*Cutl2*) exist (Neufeld et al., 1992; Quaggin et al., 1996; Tavares et al., 2000; Valarche et al., 1993). *Cux1* has been hypothesized to function in cell-cycle control, in part by regulating the G1 cyclin inhibitors $p21^{Cip1}$ and $p27^{Kip1}$ (Coqueret et al., 1998; Ledford et al., 2002), and consistent with this idea *Cux1* mutants displayed reduced growth and organ hypoplasia (Ellis et al., 2001; Luong et al., 2002; Sinclair et al., 2001), whereas *Cux1* overexpressing transgenics exhibit multiorgan hyperplasia (Ledford et al., 2002).

In contrast to *Cux1*, the role of *Cux2* remains poorly characterized, particularly in the nervous system, where it is expressed at high levels during neurogenesis (Iulianella et al., 2003; Nieto et al., 2004; Quaggin et al., 1996; Zimmer et al., 2004). *Cux2* marks interneurons in the marginal zone (mz) of the developing spinal cord (Iulianella et al., 2003) as well as progenitor cells in the subventricular zone (sz) and their descendants in the outer layers of the mouse cortex (Nieto et al., 2004; Zimmer et al., 2004). Here we reveal, through gain- and loss-of-function approaches in mouse models, novel roles for *Cux2* in regulating neurogenesis. *Cux2* directs neuroblast development and neuronal differentiation and cell-fate determination in the spinal cord by coupling cell-cycle progression in neural progenitors with differentiation through the direct activation of *Neurod and* $p27^{Kip1}$.

MATERIALS AND METHODS

Construction of full-length *Cux2* expression vectors

Full-length mouse *Cux2* cDNA was reverse transcribed from E13.5 embryo head total RNA using Superscript II Reverse Transcriptase (Invitrogen, Carlsbad, CA), oligo dT and random primers (Gene Racer Kit, Invitrogen), supplemented with mouse Cux2-specific antisense primers against the 5′ and 3′ ends of *Cux2* cDNA (GTCCTCGGGACCTGGCAGGTGGTTA and GGCAGCTGGGCCCATCATATGTTTG, respectively), using Quaggin et al. (Quaggin et al., 1996) as the reference sequence. Full-length *Cux2* cDNA was amplified using AmpliTaq Supermix (Invitrogen) and a *Cux2* 5′ sense primer (GAGCGATGGTAGCTCCGGTGCTGAA) and 3′ antisense primer (GGCAGCTGGGCCCATCATATGTTTG), allowing for sufficient time during elongation to amplify the 4.6 kb mCux2 cDNA. A 4.6 kb full-length *Cux2* cDNA was TA cloned into the TOPO PCR II vector (Invitrogen) and the entire cDNA was sequenced using a series of primers covering the full-length coding sequence. Errors in the coding sequence were corrected using the Quickchange XL kit (Stratagene, La Jolla, CA), and subcloned into pBluescript II. A Kozak consensus (GCGTAATATGGCCACAACC) was inserted immediately upstream of the *Cux2* initiating methionine using the Quickchange XL kit (Stratagene). Kozak-modified full-length cDNA was subcloned into pIRES2 bicistronic vector (Clontech, Palo Alto, CA), and the pCCAGGS bicistronic vector (Megason and McMahon, 2002) using the *Eco*RI. The pIRES2 vector is driven by the CMV intragenic enhancer and the pCCAGGS vector uses the CMV enhancer as well as β-actin promoter and intron sequences to drive robust levels of *Cux2* cDNA and green fluorescent protein (GFP) in the same cell. A double stop (TTA-TTA) was mutated (Quickchange XL, Stratagene) into the 3′ *Eco*RI site of *Cux2* cDNA in both bicistronic vectors to ensure efficient GFP translation from the bicistronic vectors.

Generation of transient *Cux2* transgenics

For neuron-specific *Cux2* expression, a 1.2 kb multimerized Nestin Intron II enhancer was amplified from pMH PICRE (a kind gift of Dr Stephen Harris) (Zimmerman et al., 1994), using a 5′ primer with an *Ase*I adaptor (CAATTAATCACAAATGCGTAAGGAGAAA) and a 3′ primer with a *Sna*BI adaptor (CATACGTACATTGTCACTCAAGTGTATG), restricted with *Ase*I and *Sna*BI and cloned into *Cux2pIRES2* bicistronic vector in which the CMV enhancer was removed with *Ase*I/*Sna*BI digestion. The transgene was linearized with *Ase*I and *Ssp*I and injected into pronuclei of FVB donor eggs to generate transient transgenic embryos. Expressors were screened using GFP fluorescence from a UV source under a Leica MZ FLIII dissecting microscope. A total of seven transient transgenic embryos was analyzed at E10.5 (n=4) and E11.5 (n=3). These embryos represent seven independent transgene integrations and displayed varying intensities of GFP expression, which correlated with the degree of neuroblast and interneuron formation (Figs 3, 6 and 7; see Fig. S2 in the supplementary material).

In ovo electroporations of chick neural tubes

Cux2-pCIG and *pCIG* (empty control vector) expression plasmids were prepared at 3–5 μg/μl concentration in water, and 0.1% Fast Green solution was added to visualize injection into HH10–12 stage chick neural tubes. Eggs were windowed and prepared for electroporation as described (Krull, 2004). Five 50 millisecond pulses of 20 volts each were applied using a CUY-21 electroporator and platinum electrodes. Eggs were re-sealed with cellophane tape and allowed to incubate for another 24–48 hours at 37°C under humidified conditions.

Generation of a *Cux2* mutant mouse line

A *Cux2* gene trap mouse embryonic stem (ES) cell line was identified by searching for Cux2 sequences in the Lexicon Genetics Omnibank library (http://www.lexicon-genetics.com/discovery/omnibank.htm). Gene trap ES clone OST440231 was identified as having a VICTR48 MTII gene trap insertion in the third intron of mouse *Cux2* gene on chromosome 5 (Fig. 2B) (Zambrowicz et al., 1998). This clone was purchased from Lexicon Genetics, thawed, expanded on feeder layers using standard ES culture procedures (Nagy et al., 2003) and injected into C57BL/6 recipient blastocysts. Two strong chimeric mice were subsequently used to generate agouti progeny carrying the gene trap insertion in the Cux2 locus.

Based on the sequence surrounding the insertion site, we developed a genotyping strategy using a primer specific to the LTR2 region of the gene trap (AAATGGCGTTACTTAAGCTAGCTTGC) and two locus-specific primers upstream and downstream of the insertion site (TGTGCCATTATGCCTCC and GTCCTTTGACCTGGCC, respectively). A 392 bp wild-type allele was amplified using the latter two primers, while a mutant allele of approximately 180 bp was generated using TGTGCCATTATGCCTCC and AAATGGCGTTACTTAAGCTAGCTTGC primers. Heterozygotes were confirmed by amplifying for the neomycin cassette present in the gene trap vector using the following primers: AACAGACAATCGGCTGCTCTG and TTCCACCATGATATTCGGCAA. *Cux2*$^{neo/+}$ were maintained on a Sv129 background and mated to generate homozygous mutant pups. The frequency of *Cux2*$^{neo/neo}$ pups was 20.5% less than expected from Mendelian segregation, indicating some prenatal lethality.

Antibody production

For *Cux2* polyclonal antibody production, a synthetic peptide (NQEKGTGEQVHSEPLS-C) derived from the C-terminal region of murine Cux-2 (amino acids 1305–1322) (Quaggin et al., 1996) was synthesized (Synpep, Dublin, CA), conjugated to KLH and used to immunize New Zealand White rabbits (Covance, Denver, PA). The resulting antisera were purified against the immunizing peptide by affinity chromatography. The antibody was used at 1/3000 dilution on frozen sections and revealed with either goat anti-rabbit Alexa Fluor 594 or goat anti-rabbit Alexa Fluor 488 (Molecular Probes/Invitrogen, Carlsbad, CA). The specificity of the anti-Cux2 antibody was examined by immunohistochemistry following Cux2 overexpression in both embryonic chick and mouse neural tubes, and in *Cux2*$^{neo/neo}$ hypomorphic neural tubes (see Fig. S3 in the supplementary material). In addition, the specific Cux2 signal in sections was abolished by incubation with a Cux2 C-terminal peptide (see above; data not shown). Also, western blots of E12.5 embryonic brains using the anti-mCux2 antibody identified an endogenously expressed doublet migrating at 110 kDa on SDS-PAGE (Fig. 2B), in agreement with the expected size for the full-length Cux2 protein.

Western blot analysis

Western blot analysis on SDS-PAGE was performed on protein extracts from E12.5 embryonic heads from two separate wild type (+/+), *Cux2*$^{neo/+}$ (+/−) and *Cux2*$^{neo/neo}$ (−/−) mutant littermates using the Cux2 polyclonal antibody we generated. Briefly, two samples from each genotype were loaded on a 7.5% polyacrylamide gel along with loading controls (BioRad, Hercules, CA), resolved using SDS-PAGE and transferred onto nitrocellulose membranes (Biorad). Blots were blocked with Odyssey blocking buffer (Licor Biosciences, Lincoln, NE) and incubated in 1/2000 dilution of the rabbit anti-Cux2 antibodies overnight at 4°C. The blot was subsequently washed with TBST, and incubated with goat anti-rabbit IRDye 800 secondary antibodies (Licor Biosciences) diluted at 1/7500 in blocking buffer at room temperature for 1–2 hours. After washes in TBST, bands were visualized using the Licor Odyssey Visualization System (Licor Biosciences). To control for sample loading,

following anti-mCux2 immunoblotting, the membrane was washed, re-blocked and then incubated in a 1/10000 dilution of anti-alpha Tubulin antibody (Sigma, St Louis, MO) at room temperate for 1 hour. Anti-alpha Tubulin signal was revealed using the SuperSignal West Pico kit (Pierce, Rockford, IL), with a brief exposure to detection film. In addition, Coomasie Blue staining of replicate polyacrylamide gels indicated approximately equal protein loading across the different samples (data not shown).

ChIP assays

Chromatin immunoprecipitation (ChIP) assays were performed using the EZ ChIP Kit (Upstate, Lake Placid, NY) according to the manufacturer's directions, with the following modifications. Brains dissected from E12.5 CD1 mice were used for ChIP analysis. The native protein-DNA complexes were cross-linked by treatment with 1% formaldehyde for 15 minutes. Briefly, equal aliquots of isolated chromatin were subjected to immunoprecipitation with an anti-Cux2, anti-RNA polymerase II or IgG antibodies. DNA associated with immunoprecipitates was used as a template for PCR analysis with primers producing a 248 bp fragment encompassing the *Neurod* promoter spanning +48 to −201, relative to the transcription start site, or with primers producing a 227 bp fragment of the $p27^{Kip1}$ promoter spanning −707 to −481, relative to the transcription start site. Primers used were: *Neurod* 5′-TACTGTGGGGGTGAGGGGAGTGGT-3′ and 3′-TGGAGCCTCGGGACACCTTGCCTT-5′, and $p27^{Kip1}$ 5′-CAGAGCAGGTTTGTTGGCAGTC-3′ and 3′-GGCTGACGAAGAAGAAGATGATTG-5′. To control for non-specific immunoprecipitation of chromatin by the Cux-2 antibody, the same DNA was used as a template for PCR analysis with primers producing a 250 bp fragment −5557 to −5308 relative to the *Neurod* transcription start site, or with primers producing a 148 bp fragment −5241 to −5094 relative to the $p27^{Kip1}$ transcription start site was performed. Primers used were: *Neurod* 5′-AGCAGAGCCTTCATCCTTCACG-3′ and 5′-TAGCAGAATCCTTCAGCCTCCCAG-3′, and $p27^{Kip1}$ 5′-TCCAGTGTGAGTTGATGCTCCTG-3′ and 5′-CAAGTCTGTGAGAAGAGAGTGTGGC-3′. Results obtained from unrelated antibody controls combined with enrichment when the Cux2 antibody is used confirmed they were in the linear range of product amplification and not a consequence of specifically immunoprecipitating chromatin.

Determination of cell-cycle parameters

Proliferation differences between $Cux2^{neo/neo}$ mutants and control wild-type littermates were assessed by counting the mitotic nuclei at E10.5 and 11.5 stained using a rabbit anti-phosphohistone H3 (pH3) antibody (Upstate) and goat anti-rabbit IgG Alexa Fluor 488 secondary antibodies (Molecular Probes/Invitrogen; Fig. 6D–E). Sections were counterstained with DAPI. Counts were made unilaterally in the medial neural tube, with pixel area being constant between control and mutant samples. The average values for each genotype and developmental stage are represented in Fig. 6F. Error bars reflect the standard deviation.

Cell-cycle parameters in $Cux2^{neo/neo}$ mutant and wild-type control E10.5 neural tubes were determined as previously described (Quinn et al., 2007). Briefly, iododeoxyuridine (IDU) was injected i.p. into E10.5 pregnant dams, followed by bromodeoxyuridine (BrdU) injection 1.5 hours later, both at 0.1 mg/kg body weight. Mice were sacrificed 2 hours following IDU injection, giving a 2 hour total pulse time for IDU and a 30 minute pulse time for BrdU. The IDU pulse-labeled nuclei in S and G2/M phases of the cell cycle in the spinal cord ventricular zone (vz) at E10.5 (Fig. 4A,B), while the BrdU pulse was just long enough to label S-phase nuclei (Fig. 4C). To detect the IDU and BrdU signals, two monoclonal anti-BrdU antibodies were used. A mouse anti-BrdU antibody from BD Transductions Labs (BD

Biosciences/Pharmingen, San Jose, CA) detects both IDU and BrdU signals, while a rat anti-BrdU antibody (Abcam, Cambridge, MA) detects only BrdU. Secondary antibodies used were chicken anti-mouse Alexa Fluor 488 and goat anti-mouse Alexa Fluor 594 (Molecular Probes/Invitrogen). The proportion of cells in S phase (Scells) and G2/M phase (Lcells) was determined as described by Quinn et al. (Quinn et al., 2007). The S-phase length (Ts) in the mouse E10.5 spinal cord was calculated using the following formula: Ts=Scells/Lcells×1.5 hours. Cell counts were conducted unilaterally on IDU- and BrdU-double-stained sections in the ventral half of the E10.5 neural tube, where Cux2 protein is normally abundant (see Fig. S1 in the supplementary material), and results are summarized as average values with standard deviation in Table 1. A total of 14 sections from three different *Cux2*$^{neo/+}$ heterozygote controls and eight sections from three different *Cux2*$^{neo/neo}$ mutant littermates were used for the analysis. Significance testing was conducted using a one-tailed Student's *t*-test with the level of significance set at <0.05.

Immunohistochemistry

Specimens were processed for cryostat and cut at 10 μm. Sections were blocked in 10% goat serum (Zymed/Invitrogen, Carlsbad, CA) for 30 minutes to 1 hour at room temperature. Primary antibodies were diluted in 10% goat serum and incubated on sections overnight at 4°C. Sections were subsequently rinsed with PBS + 0.05% Triton X-100 and incubated with the following secondary antibodies diluted at 1/250 with 10% goat serum for 1 hour: goat anti-mouse IgG Alexa Fluor 594, goat anti-mouse IgM Alexa Fluor 594, chicken anti-rabbit IgG Alexa Fluor 488, goat anti-mouse IgG Marina Blue or goat anti-guinea pig Alexa Fluor 594 (Molecular Probes/Invitrogen).

The following primary antibodies were used: Rabbit anti-Cux2 at 1/3000, mouse anti-TuJ1 at 1/500–1/1000 (Covance, Berkeley, CA), mouse anti-p27^{Kip1} at 1/200–1/300 (BD Transduction Laboratories, BD Biosciences/Pharmingen), mouse anti-NeuN at 1/500 (Chemicon, Temecula, CA), monoclonal rabbit anti-Ki67 at 1/40 (Neomarkers, LabVision, Fremont, CA), guinea pig anti-mouse Olig2 at 1/10000 (kind gift from Dr Ben Novitch, Northwestern University, Chicago, USA), guinea pig anti-Chx10 at 1/5000 (kind gift from Dr Sam Pfaff, Salk Institute, California, USA) and rabbit-anti-Neurod1 at 1/500 (kind gift of Dr Jacques Drouin, IRCM, Montreal, Canada). The following mouse monoclonal antibodies were obtained from the Developmental Studies Hybridoma Bank developed under the auspices of the NICHD and maintained by the University of Iowa, Department of Biological Sciences (Iowa City, IA 52242): Lim1/Lhx1 (4F2) at 1/50; Neurofilament (2H3) at 1/25, Isl1/2 (39.4D5) at 1/50, Nkx2.2 (74.5A5) at 1/50, Pax6 at 1/25.

For some antibodies (Ki67, Nkx2.2, HNF3β and NeuN), sections were treated for antigen retrieval using in Citrate Buffer pH 6 and a Biogenex EZ Retriever microwave set to 60°C for 10 minutes before blocking. Sections were counterstained with 1/10000 dilution of Hoechst 33342 (Molecular Probes/Invitrogen) or 1/500 dilution of 2 mg/ml DAPI (Sigma) in PBS for 5–10 minutes, followed by rinses in PBS. Slides were mounted with fluorescent mounting medium (DakoCytomation, Carpinteria, CA). All images were taken using a Ziess Axiovert 200M inverted confocal microscope with both 10× and 20× objectives, and processed using Photoshop CS2 (Adobe, San Jose, CA).

Statistics

Morphometric analysis of mouse E11.5 total neural tube area, vz and mz areas, and neural tube height and width was conducted using Axiovision's LE software (Release 4.3). The vz was delineated by Ki67-positive cells and the mz was identified either by TuJ1, p27/Kip1 or NeuN immunoreactivity. Multiple sections from four different wild-type and *Cux2*$^{neo/+}$ specimens were used as controls and were compared to multiple sections from two different

Cux2$^{neo/neo}$ mutants and four different *Cux2* transgenics. Statistical relevance was tested using a one-tailed Student's *t*-test, with the significance level set at <0.05. Differences between the *Cux2* loss-of-function and gain-of-function experiments were expressed as percentage differences between the average value from the experimental and control samples (see Table S1 in the supplementary material).

The effect of *Cux2* overexpression on TuJ1 expression in sectioned chick neural tubes was assessed by counting the number of GFP- and TuJ1-double-positive cells and expressed as a percentage of total GFP-positive cells. The effect of *Cux2* overepression was measured using seven different specimens and compared to 14 different specimens for control electroporations. Standard error was computed using regression analysis of GFP/TuJ1-double-positive versus GFP-total-positive cell numbers. Statistical significance was measured using a one-tailed Student's *t*-test with significance taken at <0.05.

The effect of *Cux2* loss and overexpression on motoneuron and interneuron formation in embryonic mouse spinal cords was assessed by counting Isl1-positive, Lhx1-positive and Chx10-positive cells in the ventral region of thoracic-level sections of E10.5 neural tubes. The pixel area used in the cell counts was kept constant between the *Cux2*$^{neo/neo}$ mutant and wild-type or heterozygous control littermates, and encompassed the entire ventral neural tube from the dorsal limit of the ventral horn to the floor plate (fp) (Fig. 7), which corresponds to the domain of high Cux2 protein expression (Fig. 1A and see Fig. S1A in the supplementary material). All counts were done unilaterally. For Isl1 counts, a total of 19 sections from eight different E10.5 wild-type and *Cux2*$^{neo/+}$ heterozygote neural tubes, 34 sections from 11 different *Cux2*$^{neo/neo}$ mutants and nine sections from four different *Nestin*-enhancer-driven *Cux2-IRES-EGFP* transgenics were used. For Lhx1, eight sections from four different E10.5 wild type, 15 sections from eight different *Cux2*$^{neo/neo}$ mutants and nine sections from four different *Cux2* transgenic embryos were used. Significant differences from controls were determined using a one-tailed Student's *t*-test with the level of significance taken at <0.05 (see Table S2 in the supplementary material). For Chx10 number, sections from forelimb regions of five different E10.5 wild type and eight different *Cux2*$^{neo/neo}$ littermates were used (Fig. 8).

RESULTS

Distribution of Cux2 in the developing spinal cord

We initially characterized the activity of Cux2 during murine spinal cord neurogenesis by profiling its distribution between E9.5 and 11.5 with a Cux2 polyclonal antibody (see Materials and methods). At E9.5, Cux2 protein was observed only in the roof plate (rp) of the neural tube and dorsal epidermis (data not shown). Interestingly, by E10.5, high levels of Cux2 protein were detected in neuronal precursors in the vz and in nascent neurons exiting the cell cycle in the intermediate zone (iz) (arrowhead in Fig. 1A) at the forelimb bud level. Importantly, *Cux2* was expressed in many proliferating progenitor cells of the vz, demarcated by S-phase nuclei that incorporated BrdU over a period of 30 minutes (Fig. 1B). Cux2 was also detected in the developing ventral interneurons of the mz, but only in the occasional cell in the ventral horn of the E10.5 spinal cord, where motoneurons are typically generated. By E11.5, Cux2 protein was abundantly detected in both the rp and fp, in progenitor cells in the vz, in nascent neurons of the iz and in post-mitotic interneurons in the mz (Fig. 1C,F,I; see Fig. S1A in the supplementary material). Interestingly, Cux2 protein was notably absent from most post-mitotic motoneuron populations in forelimb bud regions of the spinal cord (see Fig. S1A in the supplementary material). Thus Cux2 is expressed in proliferating neural progenitors and in nascent neurons (especially interneurons) during the peak phase of spinal cord neurogenesis.

The high level of Cux2 activity observed in the vz and iz was intriguing because this is the location where proliferative neuroblasts undergo cell-cycle exit and respond to signals that trigger terminal differentiation (Gui et al., 2007; Rao and Sockanathan, 2005). This implied that Cux2 might play a role in cell-cycle regulation and/or differentiation during neurogenesis. Previous work has established the importance of the Cip/Kip family of proteins in promoting cell-cycle withdrawal (Gui et al., 2007) and in particular $p27^{Kip1}$, a G1-cyclin-dependent kinase inhibitor, in regulating cycle exit and post-mitotic differentiation during spinal cord neurogenesis (Fero et al., 1996; Kiyokawa et al., 1996; Nakayama et al., 1996). $P27^{Kip1}$ protein is abundantly detected in the iz, rp and fp of E11.5 wild-type embryos (Fig. 1D,G,J; see Fig. S1B in the supplementary material). In the ventral region of the neural tube we frequently observed nuclei exiting the vz that were co-stained with $p27^{Kip1}$ and Cux2 (arrowhead, Fig. 1K). Particularly striking was the co-localization of $p27^{Kip1}$ with Cux2 (Fig. 1E,H,K; see Fig. S1C in the supplementary material) within a region of the iz 2–4 cell layers thick (Fig. 1F–H; see Fig. S1A–C in the supplementary material) that correlates with neural progenitor cells undergoing cell-cycle exit and terminal differentiation. These results suggested that Cux2 might play important roles during spinal cord neurogenesis.

Cux2 is required for neuronal development

To functionally test the role of *Cux2* during neurogenesis, we used gene trapped ES cells (Zambrowicz et al., 1998) to generate a *Cux2* mutant mouse line (Fig. 2A). $Cux2^{neo/neo}$ adults were produced at less than expected Mendelian frequency (see Materials and methods), which suggested the presence of an embryonic lethal phenotype. Western blots of E12.5 head lysates from two individual wild-type (+/+), $Cux2^{neo/+}$ (+/−) and $Cux2^{neo/neo}$ (−/−) embryos using a purified anti-mCux2 polyclonal antibody identified a doublet migrating near 110 kDa on SDS-PAGE, which was either greatly diminished or abrogated in $Cux2^{neo/neo}$ (−/−) mutants (Fig. 2B, lanes 5 and 6, respectively). The severe reduction of Cux2 protein levels in $Cux2^{neo/neo}$ embryos was confirmed by immunoprecipitation (data not shown) and immunohistochemistry (see Fig. S3G,H in the supplementary material), and indicates that the $Cux2^{neo/neo}$ gene trap mutant is a severe hypomorph.

E11.5 $Cux2^{neo/neo}$ mutant embryos exhibited hypoplastic neural tubes compared with their wild-type or heterozygous littermates at E11.5 (Fig. 2C,D). TUNEL staining revealed no significant differences in the amount of cell death between $Cux2^{neo/neo}$ mutants and control littermate neural tubes at E10.5 and 11.5 (data not shown), suggesting that loss of *Cux2* resulted in proliferation and/or differentiation deficiencies in the developing spinal cord. Histological analysis revealed that *Cux2* loss greatly affected axonal mass in the mz of the neural tube and in the ventral commissure, which preferentially stain with eosin (black arrowhead, Fig. 2D). These defects were exemplified with the definitive pan neural marker TuJ1 (neuronal-specific β-tubulin), which labels axons of post-mitotic neurons within the mz and dorsal root ganglia (drg) and clearly demarcates the boundaries of these structures (Fig. 2E,J). The domain of TuJ1 immunostaining correlating with the mz of the neural tube was much narrower throughout the entire dorsoventral extent of *Cux2* mutant embryos (Fig. 2J). Double immunostaining with Ki67 (green) and TuJ1 (red) further illustrated the preferential reduction of the differentiated mz layer in $Cux2^{neo/neo}$ mutants (Fig. 2J, compare with 2E). *Cux2* mutants exhibited a 27.8% reduction in overall neural tube area compared with controls; however, whereas the vz was diminished by 13%, the mz was 49% smaller, reflecting a preferential loss of post-mitotic populations (see Table S1 in the supplementary material). Additional defects seen in E11.5 $Cux2^{neo/neo}$ embryos included drg, which were evident by TuJ1, $p27^{Kip1}$, NeuN (Neuna60 – Mouse Genome Informatics) and Neurod immunostaining (Fig. 2J,K,M; see Fig. S2 in the supplementary material). All the post-mitotic markers examined revealed a requirement for *Cux2* function in influencing the size

of the drg, but not necessarily in the establishment of early patterning, which remained grossly intact.

Cux2 influences progenitor pool size through promoting cell-cycle length

To determine whether the neural differentiation defects observed in *Cux2* mutant embryos were primarily due to alterations in neural progenitor populations, we used Pax6 to investigate the integrity of ventral spinal cord progenitors (Fig. 3). Cux2 was co-expressed with Pax6 in ventral neural progenitors at E10.5 and 11.5 (data not shown). In comparison to wild type, *Cux2* mutant embryos exhibited a mediolateral reduction in Pax6-positive nuclei in the neural tube at E11.5 (Fig. 3A,B), demonstrating a requirement for *Cux2* in the formation and/or maintenance of spinal cord progenitors.

Given the requirement for *Cux2* function in spinal cord progenitors, we next evaluated the progression of the cell cycle in the vz cells of E10.5 embryos via sequential pulsing of neural progenitors with IDU and BrdU as previously described (Quinn et al., 2007). Briefly, the G2/M phase of the cell cycle was labeled through a 2 hour pulse with IDU (green/yellow in Fig. 4A,C), while the proliferating nuclei localized to the lateral half of the vz were labeled by a 30 minute pulse with BrdU (red/yellow in Fig. 4A). By counting the number of nuclei in S phase (called *Scells*; i.e. BrdU/IDU co-labeled cells, Fig. 4A) and comparing it to the number of nuclei that have left S phase (called *Lcells*; i.e. IDU label alone, Fig. 4A), the S-phase length (called *Ts*) can be determined (Fig. 4C). $Cux2^{neo/neo}$ mutants (n=8) displayed a significantly greater number of nuclei in S phase, and a reduced number of nuclei in G2/M phase (i.e. nuclei that have left the S phase) relative to controls (n=14; Fig. 4B; Table 1). This resulted in a significant 62% increase in neural progenitor S-phase length in $Cux2^{neo/neo}$ mutant embryos relative to controls (P=0.0001, Table 1), and reflected a slowing of the cell cycle in *Cux2* mutants.

To determine if the alteration of cell-cycle dynamics in the *Cux2* mutants affected neural progenitor proliferation, we examined the number of neuroepithelial mitoses in $Cux2^{neo/neo}$ and control littermates. Anti-pH3 antibodies labeled mitotic nuclei at the luminal edge of the vz (green, Fig. 4D,E). At E10.5, proliferation levels were comparable between $Cux2^{neo/neo}$ mutants (n=18) and control (n=9) littermates (Fig. 4F). However, by E11.5 the *Cux2* hypomorphs (n=5) displayed significantly reduced pH3 staining (P=0.009) relative to littermate controls (n=6; Fig. 4F). Thus the reduced G2/M progression observed in the *Cux2* mutants at E10.5 resulted in reduced proliferation by E11.5. This correlates with the onset and peak temporal period of Cux2 activity (Fig. 1) and can account for the mediolateral reduction in Pax6-positive progenitors observed at the same developmental stage. A consequence of slowing down the cell-cycle progression in the vz progenitors is decreased post-mitotic neurons in the mz, and indeed TuJ1 immunostaining illustrated the greatly reduced mz in $Cux2^{neo/neo}$ mutant embryos (Fig. 2E,J).

Cux2 is required for cell-cycle exit and neuronal differentiation

The effect of Cux2 on Pax6-positive neural progenitors raised the possibility that *Cux2* influences the formation of neuroblasts. Here we define neuroblasts as migratory immature neuronal descendants of progenitor cells that express basic helix-loop-helix (bHLH) proteins such as Neurod1 (Lee et al., 2000). Interestingly, Neurod promotes neuronal differentiation in part through the activation of $p27^{Kip1}$ (Farah et al., 2000; Lee et al., 1995), and $p27^{Kip1}$ is upregulated and co-expressed with *Cux2* in the iz, which corresponds with cell-cycle withdrawal and terminal differentiation of neural progenitors (Fig. 1C–K, Fig. 2F,G; see Fig. S1A–C in the supplementary material). We therefore assessed whether the reduction in the size of the differentiated mz layer in *Cux2* mutants embryos was due to specific effects on Neurod and $p27^{Kip1}$.

We initially examined the relationship between Neurod1 and $p27^{Kip1}$ in the developing spinal cord (see Fig. S4 in the supplementary material). At E9.5, Neurod1-positive nuclei were detected at the lateral edges of the vz in a pattern that was mostly non-overlapping with $p27^{Kip}$-labeled cells (see Fig. S4A in the supplementary material). The occasional co-labeled nuclei were detected in ventral pseudostratified neuroepithelium (arrow in Fig. S4A in the supplementary material). By E10.5, the bulk of Neurod-positive neuroblasts resided in the vz immediately adjacent to $p27^{Kip1}$-positive post-mitotic neurons in the iz and mz (Fig. 3I; see Fig. S4C in the supplementary material), indicating that the activity of Neurod1 and $p27^{Kip}$ are largely independent of one another. However, small numbers of Neurod1/$p27^{Kip1}$-double-positive cells were observed in the iz (arrow, Fig. 3I; see Fig. S4C in the supplementary material). These double-labeled cells were neuroblasts withdrawing from the cell cycle and undergoing terminal differentiation. Neurod1 levels were only modestly attenuated in E9.5 $Cux2^{neo/neo}$ mutants (see Fig. S4 in the supplementary material). By contrast, E10.5 $Cux2^{neo/neo}$ mutant embryos exhibited a striking reduction of Neurod-labeled cells (Fig. 3J; see Fig. S4D in the supplementary material). E11.5 wild-type embryos expressed Neurod1 specifically in neuroblasts located within the ventral half of the neural tube and at the lateral edge of the vz (Fig. 3E), and the severe reduction of Neurod1 expression at this stage in *Cux2* mutants highlighted their deficient ability to generate neuroblasts (Fig. 3F).

In comparison with Neurod1, a greater reduction of $p27^{Kip1}$ was observed upon *Cux2* loss at E9.5 (see Fig. S4B in the supplementary material). Furthermore, fewer $p27^{Kip1}$-expressing cells were also observed in the iz of $Cux2^{neo/neo}$ mutants at E10.5 relative to controls (arrow, Fig. 3J; see Fig. S4D in the supplementary material). By E11.5, the effect of *Cux2* loss on $p27^{Kip1}$-expressing cells in the iz was even more pronounced (Fig. 2F,K,G,L). Thus, *Cux2* loss attenuated the formation of neuroblasts and also affected their exit from the cell cycle. Collectively, these results indicate that the reduction in spinal cord size in $Cux2^{neo/neo}$ embryos was not simply the result of alterations in the progenitor pool size, but also reflected a requirement for *Cux2* in neuroblast formation and differentiation.

Cux2 is present in activator complexes bound to the native promoters of *Neurod1* and $p27^{Kip1}$

Our *Cux2* loss-of-function analyses highlighted both Neurod1 and $p27^{Kip1}$ as potential direct targets of Cux2 during neurogenesis. To directly assess if Cux2 interacts with the native *Neurod1* and $p27^{Kip1}$ promoters, we performed ChIP analysis using chromatin isolated from brains of E12.5 embryos, a tissue that normally expresses high levels of Cux2. The ChIP assays were carried out using IgG (negative control), anti-Cux2 and anti-polymerase II (positive control) antibodies. We focused on the proximal regions of the *Neurod1* and $p27^{Kip1}$ promoters, which have several putative AT-rich *Cux*-binding sites. A clear PCR product for *Neurod1* was observed in the high concentration anti-Cux2 ChIP (Fig. 5A, lane 10). Similarly, a PCR product for $p27^{Kip1}$ was detected in both the high and low concentration of anti-Cux2 ChIP (Fig. 5C, lanes 9 and 10). In control experiments, amplification of sequences 5 kb upstream from the *Neurod1* (Fig. 5B) or $p27^{Kip1}$ (Fig. 5D) transcription start sites produced no Cux2-bound products. These results clearly show that Cux2 is part of a complex bound to the *Neurod1* and $p27^{Kip1}$ promoters in their native chromatin configuration. Therefore, *Neurod1* and $p27^{Kip1}$ are direct in vivo transcriptional targets of Cux2, which mechanistically accounts for the functional properties of *Cux2* in regulating neuroblast formation and cell-cycle exit during mammalian spinal cord neurogenesis.

Cux2 overexpression results in enlarge neural tubes and enhanced neurogenesis

To further validate a requirement for *Cux2* during spinal cord neurogenesis, we investigated the effect of overexpressing *Cux2* in neural progenitors via mouse transgenesis using the *Nestin* intron II enhancer (Zimmerman et al., 1994). We were unable to obtain postnatal *Nestin-Cux2-ires-EGFP*-expressing transgenics due to late gestation embryonic lethality and therefore restricted our analyses to transient transgenic embryos at E10.5–11.5. Seven independent integrants appropriately expressing high levels of GFP and thus Cux2 protein in neural progenitors were selected for analysis (see Fig. S3 in the supplementary material). *Cux2* transgenic embryos consistently exhibited modest increases in total neural tube size (11% larger than controls), with the mz being preferentially affected relative to the vz (14 versus 8% respectively; see Table S1 in the supplementary material). These observations complemented the *Cux2* mutant phenotype and indicated that Cux2 regulates spinal cord neurogenesis.

We next used Pax6 to investigate neural progenitor development within the ventral domain of E11.5 spinal cords (Fig. 3). In comparison with wild-type littermates, *Cux2* transgenic embryos displayed a mediolateral expansion of Pax6-positive progenitor cells (arrows, Fig. 3C,D), but no dorsoventral expansion, despite strong GFP expression throughout the entire extent of the neural tube. These results contrast well with the reduction in Pax6 progenitors observed in stage-matched *Cux2* mutants. Thus Cux2 dosage is an important regulator of progenitor pool size.

Given that Cux2 binds to the proximal promoters of *Neurod1* and *p27^{Kip1}*, we examined the effect of manipulating Cux2 levels on the formation of neuroblasts and p27^{Kip1}-mediated cell-cycle exit. *Cux2* mutants displayed a severe reduction in Neurod1-positive neuroblasts relative to wild-type controls (Fig. 3E,F). By contrast, *Cux2* overexpression dramatically enhanced neuroblast formation in a cell-autonomous manner in the spinal cord of E10.5 and 11.5 embryos (Fig. 3G–L). Neurod-positive cells are normally found only within the lateral domain of the vz and not in the most apical portion, where progenitor cells reside (Fig. 3E). Although *Cux2* overexpression enhanced Neurod1-positive neuroblast formation, it did so only in the lateral domain of the vz and did not force the apical progenitor cells to ectopically adopt a neuroblast fate. This may explain why Cux2 overexpression did not automatically lead to a premature depletion of the stem cell pool.

Our *Cux2* mutant analyses and ChiP assays uncovered *p27^{Kip1}* and *Neurod1* as important downstream targets of Cux2 that are crucial for cell-cycle exit. We therefore analyzed E11.5 *Cux2*-overexpressing transients for markers of post-mitotic neurons and definitive neurogenesis. In control embryos, p27^{Kip1} activity is prominently expressed in the iz, corresponding with neural progenitor cell-cycle exit and terminal differentiation (Fig. 6A). *Cux2* overexpression in neural progenitors induced high levels of p27^{Kip1} activity in cells in the iz and mz, and to a lesser extent in the vz (Fig. 6B,C). Taken together with the co-localization of Cux2 and p27^{Kip1}, this supports the argument in favor of a role for Cux2 in regulating cell-cycle exit of neuronal precursors.

Cux2 transgenic embryos displayed ectopic NeuN (Fig. 6E,F, versus 6D), neurofilament (Fig. 6H,I, compare with G) and TuJ1 staining (data not shown) throughout the mz of the spinal cord, consistent with an enhancement of neurogenesis. Surprisingly, many of the axon filaments appeared to be disorganized, projecting laterally instead of ventrally (Fig. 6H,I versus 6G). This suggested that *Cux2* not only enhanced neural differentiation but also influenced neuronal migration, maturation and/or patterning. Importantly, the markers of post-mitotic neurons (e.g. NeuN and neurofilament) were not ectopically activated in the vz of *Cux2* transgenics, despite strong *Cux2-GFP* expression there (Fig. 6D–I). Thus even though Cux2 promotes cell-cycle exit and interneuron formation, it is not at the expense of

transforming all of the neural stem or progenitor cells prematurely into post-mitotic neurons. This is consistent with the exit of quiescent cell populations from the proliferative vz occurring before neuronal maturation (Fig. 6) (Gui et al., 2007).

In an effort to quantify the effect of *Cux2* on neurogenesis, we constitutively overexpressed *Cux2* in the neural tube of HH7–8-stage chick embryos via in ovo electroporation and analyzed the embryos with TuJ1 immunostaining 24 hours later. In *Cux2-ires-EGFP* electroporated neural tubes, 14.2% of Cux2/GFP labeled cells were also TuJ1 positive (n=7; Fig. 6J–L). By contrast, in control electroporated neural tubes, only 5.8% of GFP-labeled cells were TuJ1 positive (n=14; Fig. 6L). Our results therefore demonstrate that Cux2 acts as an important regulator of neural differentiation throughout the developing spinal cord.

Cux2 regulates ventral interneuron and motoneuron formation

Cux2 mutant spinal cords displayed a strikingly specific reduction of $p27^{Kip1}$ in the iz and mz (arrowhead, Fig. 2L versus 2G) but surprisingly not in the ventrolateral motoneuron domain (Fig. 2K, compare with 2F). These results were suggestive of a selective loss of interneurons in $Cux2^{neo/neo}$ mutant embryos and indicated that *Cux2* may upregulate $p27^{Kip1}$ in neural progenitors to force their exit from the cell cycle and initiate differentiation. Further evidence supporting selective interneuron loss came from analyses of the levels of the phosphoprotein NeuN (Lind et al., 2005). NeuN demarcates mature post-mitotic neurons and is initially observed in the ventral motoneuron population before expanding to dorsal neuron populations in conjunction with ventral to dorsal maturation of the spinal cord (Mullen et al., 1992). We observed that NeuN immunostaining was more intense in the lateral motoneuron domain of *Cux2* mutant embryo spinal cords compared with wild-type littermates (Fig. 2M–N versus 2H–I). This implied that the loss of *Cux2* led to an increase in the formation of motoneurons and suggested that *Cux2* normally acts as a cell-fate determinant by promoting interneuron formation and limiting motoneuron generation.

To better substantiate a functional role for *Cux2* in fate determination, we characterized the pattern of interneuron and motoneuron development in our gain- and loss-of-function models (Fig. 7). Lhx1 labels ventral interneuron populations (v1, v2) at E10.5 (Fig. 7A) (Tsuchida et al., 1994) and $Cux2^{neo/neo}$ mutants (n=15) displayed a significant decrease (16%, P=0.007) in Lhx1-positive neurons in the ventral neural tube (Fig. 7B,N; see Table S2 in the supplementary material). We next examined the expression of Chx10 protein, a homeodomain transcription factor, in V2 interneurons (Fig. 8). Loss of *Cux2* led to a significant reduction of Chx10-positive cells in the ventral spinal cord at E10.5 (Fig. 8B). Quantification of Chx10-positive cells in $Cux2^{neo/neo}$ mutants (n=8) revealed a 45% reduction (P=0.002) relative to control littermates (n=5). Collectively this supports the argument for a role for Cux2 in promoting interneuron development.

Fate-mapping studies have demonstrated that Olig2 progenitors give rise to motoneurons (Masahira et al., 2006; Mukouyama et al., 2006), whereas Nkx2.2 labels the ventral most progenitor domain in the neural tube that contributes to the formation of v3 interneurons (Briscoe et al., 1999). We used Olig2 in combination with Isl1/2 to characterize progenitor and post-mitotic motoneuron patterning (Fig. 7E,F) and Nkx2.2 to identify v3 progenitors (Fig. 7I,J) (Mizuguchi et al., 2001; Novitch et al., 2001). E10.5 $Cux2^{neo/neo}$ mutant embryos displayed an expansion of Olig2-positive motoneuron progenitors (Fig. 7F) and a concomitant reduction in the dorsal extent of the Nkx2.2 progenitor domain (Fig. 7J). This correlated with an increase in Isl1/2-positive motoneurons at the ventrolateral margin of the spinal cord (n=11; Fig. 7F; see Table S2 in the supplementary material). These effects were independent of any alterations of Shh levels in the ventral neural tube, which were comparable between E10.5 $Cux2^{neo/neo}$ mutants and control littermates (data not shown). Quantification of the effect of *Cux2* loss revealed a highly significant (P<0.001) 32%

increase in Isl1/2-positive motoneurons (*n*=11, Fig. 7M; see Table S2 in the supplementary material), demonstrating that Cux2 normally acts to limit motoneuron formation. Taken together, these results indicate that Cux2 acts as a cell-fate determinant, promoting the generation of interneurons but limiting motoneuron development.

Cux2 overexpression promotes ventral interneuron but not motoneuron formation

Given the sensitivity of neurogenesis to *Cux2* gene dosage, we next examined whether *Cux2* gain of function impacted on cell-fate determination in a complementary fashion to *Cux2* mutants (Fig. 7). *Cux2* overexpression resulted in an increase in Lhx1-positive ventral interneurons (*n*=4, Fig. 7C,D; see Table S2 in the supplementary material), indicating that Cux2 can indeed promote interneuron formation. We quantified this effect and observed that *Cux2* overexpression in neural progenitors led to a 43% increase (*P*=0.0058) in the formation of ventral interneurons (*n*=4; Fig. 7N; see Table S2 in the supplementary material). This result was complementary to that obtained in isochronic $Cux2^{neo/neo}$ mutants, which displayed a significant loss of Lhx1-positive neurons (Fig. 7N; see Table S2 in the supplementary material). Furthermore, a comparison of *Cux2* mutants to transgenic embryos revealed 70% fewer (*P*=0.007) Lhx1-positive cells (Fig. 7N; see Table S2 in the supplementary material), supporting a role for Cux2 in promoting interneuron development.

Lastly, we evaluated the effect of *Cux2* gain of function on the formation of motoneurons. *Cux2* overexpression in ventral progenitors led to a 20% decrease (*P*=0.0053) in Isl1/2-positive motoneurons in the ventrolateral margin of the spinal cord relative to littermate controls (*n*=4, Fig. 7G,H; see Table S2 in the supplementary material). By contrast, as described above, *Cux2* loss resulted in a 32% increase in Isl1/2-positive motoneurons (*n*=11, Fig. 7M; see Table S2 in the supplementary material). The effects on motoneuron formation were even more pronounced when gain- and loss-of function embryos were compared. A highly significant increase (61%) in motoneuron production was observed in the $Cux2^{neo/neo}$ mutants relative to *Cux2* transgenics (*P*<0.001; Fig. 7M; see Table S2 in the supplementary material). These results further illustrate a cell-fate determinant function for *Cux2* during spinal cord neurogenesis.

DISCUSSION

The acquisition of cell-type-specific neuronal fate is coupled to the differentiation of neural precursors in vertebrates (Cremisi et al., 2003; Ohnuma et al., 2002); however, the nature of the intrinsic signals that integrate cell-cycle control with these processes during neurogenesis remain rudimentary. Our results demonstrate that *Cux2* is an important mediator of spinal cord neurogenesis, acting through the direct regulation of the proneural gene *Neurod* and cell-cycle inhibitor $p27^{Kip1}$ in spinal cord progenitors. We show for the first time that a single factor, *Cux2*, can promote both progression of cell cycle in neural progenitors and stimulate neuronal differentiation in the developing mammalian spinal cord. *Cux2* mouse mutants exhibited fewer Pax6-, Chx10- and Nkx2.2-positive progenitors, diminished neuroblast formation and $p27^{Kip1}$-driven cell-cycle exit correlating with a loss of ventral interneurons. However, not all post-mitotic neurons were decreased, as we noted a surprising enhancement of motoneuron formation preceded by an expansion of the olig2-positive motoneuron progenitor domain. Interestingly, Cux2 is expressed in post-mitotic interneurons but is conspicuously weak or absent from the lateral motoneuron domain. Given that Shh protein levels remained robust in the *Cux2* hypomorphs, this supports the argument that Cux2 directly influences the acquisition of cell fate in ventral progenitors of the developing spinal cord and may normally act to promote interneuron formation at the expense of motoneurons.

It is possible that the enhanced formation of motoneurons in the *Cux2* mutants may be due to changes in neural progenitor cycle length. The generation of different types of neurons in the central nervous system has been purported to be influenced in part by the length of the cell cycle, which progressively increases during embryogenesis (Durand et al., 1998; Gao et al., 1997; Raff et al., 1998; Shen et al., 2006; Wilcock et al., 2007), and furthermore, interneuron generation commences before motoneuron formation in the spinal cord (Sechrist and Bronner-Fraser, 1991). We documented a significant lengthening of the S phase in the spinal cord progenitors of *Cux2* mutants, suggesting that Cux2 influences the balance of interneurons and motoneurons at least in part by regulating the length of the progenitor cell cycle. In agreement with these observations, overexpressing *Cux2* in the vz of the developing neural tube enhanced progenitor development and promoted Neurod1-positive neuroblast formation and $p27^{Kip1}$-driven cell-cycle exit. As a result, neurogenesis was enhanced, particularly with respect to the formation of interneurons. Importantly, using ChIP assays from embryonic brain extracts we determined that the regulation of *Neurod1* and $p27^{Kip1}$ by Cux2 was direct, as Cux2 bound the transcriptionally active proximal promoters of these genes. Although neurogenesis defects have been reported for *Neurod1* null mutants (Goebbels et al., 2005; Liu et al., 2000; Miyata et al., 1999), no spinal cord defects have been reported, perhaps reflecting redundancy with other widely expressed bHLH factors (Helms et al., 2005; McCormick et al., 1996). Similarly, whereas $p27^{Kip1}$ appears to be dispensable for spinal cord neurogenesis, $p27^{Kip1}/p57^{Kip2}$ double mutants show defects in cell-cycle exit of neuronal progenitors, which are associated with reduced formation of ventral interneurons (Gui et al., 2007). This phenotype is reminiscent of the $Cux2^{neo/neo}$ mutant described here. For both Neurod1 and $p27^{Kip1}$, altering Cux2 levels genetically in spinal cord progenitors led to dramatic alterations in the expression of these key neurogenic factors, particularly in nascent neurons undergoing cell-cycle exit. Whether Neurod1 regulates $p27^{Kip1}$ also remains a possibility, as there is limited co-expression in nascent neurons from E9.5 onwards. However, recent work has demonstrated that $p27^{Kip1}$ engages neurogenesis by promoting cell-cycle exit and stabilization of proneural proteins (Nguyen et al., 2006). Thus, Cux2-mediated upregulation of $p27^{Kip1}$ in the iz may also promote neurogenesis by maintaining robust bHLH gene expression in neuroblasts exiting the cell cycle, thereby accounting for the relative specificity of *Cux2* mutant phenotype. Our findings thus establish for the first time the importance a Cut homeodomain transcription factor in a genetic hierarchy acting upstream of a bHLH neurogenic factor during vertebrate neurogenesis.

In the current study, we show that Cux2 is crucial in establishing and/or maintaining the spinal cord progenitor pool. Importantly, individual cells within the undifferentiated neuroepithelium are not necessarily equivalent, and only some cells have neuron-generating potential (Wilcock et al., 2007). These so-called neurogenic cells divide to generate a progenitor and a neuron and as such influence patterning and development of both the vz and iz/mz. In *Cux2* gain- and loss-of-function embryos, we observed complementary alterations to both progenitor and differentiated neuronal populations, implying that Cux2 may impart neurogenic potential to undifferentiated neuroepithelial cells. It is perhaps in these populations that the loss of *Cux2* is most acutely felt. Cux2 therefore appears to be required for both neural progenitor maintenance and neural differentiation. Given that these two processes are often viewed as antagonistic (Bylund et al., 2003), how is it that Cux2 activity can regulate both the formation and/or maintenance of neural progenitors and neural differentiation? One possible explanation is that Cux2 acts through separate mechanisms on the distinct cell states of the developing spinal cord. Alternatively, Cux2 may function as a key regulator of the cell cycle in both neural progenitors and nascent neurons. In neural progenitors, Cux2 seems to be required for proper G2/M transition, while in nascent neurons Cux2 stimulates terminal cell division and promotes $p27^{Kip1}$-mediated cell-cycle withdrawal

(Fig. 9). Cux2 activity can therefore promote both progenitor divisions and the formation of newly born neurons.

Therefore, based on the complementary gain- and loss-of-function experiments presented here, we propose the following model describing the role of *Cux2* in spinal cord neurogenesis (Fig. 9). In the spinal cord vz, Cux2 expression promotes and/or maintains the Pax6-positive progenitor pool by promoting the progression of the cell cycle. Cux2 also directly stimulates neuroblast formation by activating proneural genes such as *Neurod*. Within the iz, these neuroblasts undergo cell-cycle withdrawal in response to high levels of $p27^{Kip1}$, which is in turn activated by high levels of Cux2. This terminal cell division cycle then generates nascent post-mitotic interneurons, which migrate to their final destinations in the lateral edges of the spinal cord.

In conclusion, our findings have uncovered for the first time multiple functional roles for a *Cut-like* homeodomain transcription factor in regulating key aspects of spinal cord neurogenesis. *Cux2* integrates cell-cycle progression with neural progenitor differentiation and cell-fate determination. Future work involving global proteomic analyses aimed at identifying the complete set of Cux2 interacting partners will be essential to fully understand how Cux2 elicits its multiple functions during neurogenesis. Subsequently it will be very interesting to extend these findings not only to spinal cord development but also to the mammalian cortex, where *Cux* genes demarcate specific upper layers of cortical neurons (II–IV) and may have played a role in the expansion and increased complexity of the cortex during evolution.

Supplementary Material

Refer to Web version on PubMed Central for supplementary material.

Acknowledgments

We are grateful for the assistance and advice of Teri Johnson, Sharon Beckham and Jean-Philippe Rey in the Histology Core Facility, Mike Elmore and Mike Morgan in Laboratory Animal Services for the generation and maintenance of mutant mouse lines, Stephanie Kong for advice and protocols regarding western blots, and Drs Ron Yu, Juan Bruses and Christof Nolte for the critical reading of the manuscript. A.I. is a recipient of a post-doctoral fellowship from the Canadian Institutes of Heath Research. G.B.V. is supported a grant from the National Institute of Diabetes and Digestive and Kidney Diseases (DK-058377). P.A.T. is supported by funding from the Stowers Institute for Medical Research, the March of Dimes (6FY05-82), the National Institute of Dental and Craniofacial Research (RO1 DE 016082-01) and the Hudson Foundation.

References

Androutsellis-Theotokis A, Leker RR, Soldner F, Hoeppner DJ, Ravin R, Poser SW, Rueger MA, Bae SK, Kittappa R, McKay RD. Notch signalling regulates stem cell numbers in vitro and in vivo. Nature. 2006; 442:823–826. [PubMed: 16799564]

Blochlinger K, Bodmer R, Jan LY, Jan YN. Patterns of expression of cut, a protein required for external sensory organ development in wild-type and cut mutant Drosophila embryos. Genes Dev. 1990; 4:1322–1331. [PubMed: 1977661]

Blochlinger K, Jan LY, Jan YN. Transformation of sensory organ identity by ectopic expression of Cut in Drosophila. Genes Dev. 1991; 5:1124–1135. [PubMed: 1676691]

Bodmer R, Barbel S, Sheperd S, Jack JW, Jan LY, Jan YN. Transformation of sensory organs by mutations of the cut locus of D. melanogaster. Cell. 1987; 51:293–307. [PubMed: 3117374]

Briscoe J, Sussel L, Serup P, Hartigan-O'Connor D, Jessell TM, Rubenstein JL, Ericson J. Homeobox gene Nkx2.2 and specification of neuronal identity by graded Sonic hedgehog signalling. Nature. 1999; 398:622–627. [PubMed: 10217145]

Bylund M, Andersson E, Novitch BG, Muhr J. Vertebrate neurogenesis is counteracted by Sox1–3 activity. Nat. Neurosci. 2003; 6:1162–1168. [PubMed: 14517545]

Coqueret O, Berube G, Nepveu A. The mammalian Cut homeodomain protein functions as a cell-cycle-dependent transcriptional repressor which downmodulates p21WAF1/CIP1/SDI1 in S phase. EMBO J. 1998; 17:4680–4694. [PubMed: 9707427]

Cremisi F, Philpott A, Ohnuma S. Cell cycle and cell fate interactions in neural development. Curr. Opin. Neurobiol. 2003; 13:26–33. [PubMed: 12593979]

Durand B, Raff M. A cell-intrinsic timer that operates during oligodendrocyte development. BioEssays. 2000; 22:64–71. [PubMed: 10649292]

Durand B, Fero ML, Roberts JM, Raff MC. p27Kip1 alters the response of cells to mitogen and is part of a cell-intrinsic timer that arrests the cell cycle and initiates differentiation. Curr. Biol. 1998; 8:431–440. [PubMed: 9550698]

Ellis T, Gambardella L, Horcher M, Tschanz S, Capol J, Bertram P, Jochum W, Barrandon Y, Busslinger M. The transcriptional repressor CDP (Cutl1) is essential for epithelial cell differentiation of the lung and the hair follicle. Genes Dev. 2001; 15:2307–2319. [PubMed: 11544187]

Farah MH, Olson JM, Sucic HB, Hume RI, Tapscott SJ, Turner DL. Generation of neurons by transient expression of neural bHLH proteins in mammalian cells. Development. 2000; 127:693–702. [PubMed: 10648228]

Fero ML, Rivkin M, Tasch M, Porter P, Carow CE, Firpo E, Polyak K, Tsai LH, Broudy V, Perlmutter RM, et al. A syndrome of multiorgan hyperplasia with features of gigantism, tumorigenesis, and female sterility in p27(Kip1)-deficient mice. Cell. 1996; 85:733–744. [PubMed: 8646781]

Gao FB, Durand B, Raff M. Oligodendrocyte precursor cells count time but not cell divisions before differentiation. Curr. Biol. 1997; 7:152–155. [PubMed: 9016704]

Goebbels S, Bode U, Pieper A, Funfschilling U, Schwab MH, Nave KA. Cre/loxP-mediated inactivation of the bHLH transcription factor gene NeuroD/BETA2. Genesis. 2005; 42:247–252. [PubMed: 16028233]

Gui H, Li S, Matise MP. A cell-autonomous requirement for Cip/Kip cyclin-kinase inhibitors in regulating neuronal cell cycle exit but not differentiation in the developing spinal cord. Dev. Biol. 2007; 301:14–26. [PubMed: 17123502]

Helms AW, Battiste J, Henke RM, Nakada Y, Simplicio N, Guillemot F, Johnson JE. Sequential roles for Mash1 and Ngn2 in the generation of dorsal spinal cord interneurons. Development. 2005; 132:2709–2719. [PubMed: 15901662]

Iulianella A, Vanden Heuvel G, Trainor P. Dynamic expression of murine Cux2 in craniofacial, limb, urogenital and neuronal primordia. Gene Expr. Patterns. 2003; 3:571–577. [PubMed: 12971989]

Jessell TM. Neuronal specification in the spinal cord: inductive signals and transcriptional codes. Nat. Rev. Genet. 2000; 1:20–29. [PubMed: 11262869]

Kintner C. Neurogenesis in embryos and in adult neural stem cells. J. Neurosci. 2002; 22:639–643. [PubMed: 11826093]

Kiyokawa H, Kineman RD, Manova-Todorova KO, Soares VC, Hoffman ES, Ono M, Khanam D, Hayday AC, Frohman LA, Koff A. Enhanced growth of mice lacking the cyclin-dependent kinase inhibitor function of p27(Kip1). Cell. 1996; 85:721–732. [PubMed: 8646780]

Krull CE. A primer on using in ovo electroporation to analyze gene function. Dev. Dyn. 2004; 229:433–439. [PubMed: 14991698]

Ledford AW, Brantley JG, Kemeny G, Foreman TL, Quaggin SE, Igarashi P, Oberhaus SM, Rodova M, Calvet JP, Vanden Heuvel GB. Deregulated expression of the homeobox gene Cux-1 in transgenic mice results in downregulation of p27(kip1) expression during nephrogenesis, glomerular abnormalities, and multiorgan hyperplasia. Dev. Biol. 2002; 245:157–171. [PubMed: 11969263]

Lee JE, Hollenberg SM, Snider L, Turner DL, Lipnick N, Weintraub H. Conversion of Xenopus ectoderm into neurons by NeuroD, a basic helix-loop-helix protein. Science. 1995; 268:836–844. [PubMed: 7754368]

Lee JK, Cho JH, Hwang WS, Lee YD, Reu DS, Suh-Kim H. Expression of neuroD/BETA2 in mitotic and postmitotic neuronal cells during the development of nervous system. Dev. Dyn. 2000; 217:361–367. [PubMed: 10767080]

Lind D, Franken S, Kappler J, Jankowski J, Schilling K. Characterization of the neuronal marker NeuN as a multiply phosphorylated antigen with discrete subcellular localization. J. Neurosci. Res. 2005; 79:295–302. [PubMed: 15605376]

Liu M, Pleasure SJ, Collins AE, Noebels JL, Naya FJ, Tsai MJ, Lowenstein DH. Loss of BETA2/NeuroD leads to malformation of the dentate gyrus and epilepsy. Proc. Natl. Acad. Sci. USA. 2000; 97:865–870. [PubMed: 10639171]

Luong MX, van der Meijden CM, Xing D, Hesselton R, Monuki ES, Jones SN, Lian JB, Stein JL, Stein GS, Neufeld EJ, et al. Genetic ablation of the CDP/Cux protein C terminus results in hair cycle defects and reduced male fertility. Mol. Cell. Biol. 2002; 22:1424–1437. [PubMed: 11839809]

Lupo G, Harris WA, Lewis KE. Mechanisms of ventral patterning in the vertebrate nervous system. Nat. Rev. Neurosci. 2006; 7:103–114. [PubMed: 16429120]

Masahira N, Takebayashi H, Ono K, Watanabe K, Ding L, Furusho M, Ogawa Y, Nabeshima Y, Alvarez-Buylla A, Shimizu K, et al. Olig2-positive progenitors in the embryonic spinal cord give rise not only to motoneurons and oligodendrocytes, but also to a subset of astrocytes and ependymal cells. Dev. Biol. 2006; 293:358–369. [PubMed: 16581057]

McConnell SK. Constructing the cerebral cortex: neurogenesis and fate determination. Neuron. 1995; 15:761–768. [PubMed: 7576626]

McCormick MB, Tamimi RM, Snider L, Asakura A, Bergstrom D, Tapscott SJ. NeuroD2 and neuroD3: distinct expression patterns and transcriptional activation potentials within the neuroD gene family. Mol. Cell. Biol. 1996; 16:5792–5800. [PubMed: 8816493]

Megason SG, McMahon AP. A mitogen gradient of dorsal midline Wnts organizes growth in the CNS. Development. 2002; 129:2087–2098. [PubMed: 11959819]

Miyata T, Maeda T, Lee JE. NeuroD is required for differentiation of the granule cells in the cerebellum and hippocampus. Genes Dev. 1999; 13:1647–1652. [PubMed: 10398678]

Mizuguchi R, Sugimori M, Takebayashi H, Kosako H, Nagao M, Yoshida S, Nabeshima Y, Shimamura K, Nakafuku M. Combinatorial roles of olig2 and neurogenin2 in the coordinated induction of pan-neuronal and subtype-specific properties of motoneurons. Neuron. 2001; 31:757–771. [PubMed: 11567615]

Mizuguchi R, Kriks S, Cordes R, Gossler A, Ma Q, Goulding M. Ascl1 and Gsh1/2 control inhibitory and excitatory cell fate in spinal sensory interneurons. Nat. Neurosci. 2006; 9:770–778. [PubMed: 16715081]

Mukouyama YS, Deneen B, Lukaszewicz A, Novitch BG, Wichterle H, Jessell TM, Anderson DJ. Olig2+ neuroepithelial motoneuron progenitors are not multipotent stem cells in vivo. Proc. Natl. Acad. Sci. USA. 2006; 103:1551–1556. [PubMed: 16432183]

Mullen RJ, Buck CR, Smith AM. NeuN, a neuronal specific nuclear protein in vertebrates. Development. 1992; 116:201–211. [PubMed: 1483388]

Nagy, A.; Gertsenstein, M.; Vintersten, K.; Behringer, RR. Manipulating the Mouse Embryo. Cold Spring Harbor Laboratory; Cold Spring Harbor: 2003.

Nakayama K, Ishida N, Shirane M, Inomata A, Inoue T, Shishido N, Horii I, Loh DY. Mice lacking p27(Kip1) display increased body size, multiple organ hyperplasia, retinal dysplasia, and pituitary tumors. Cell. 1996; 85:707–720. [PubMed: 8646779]

Neufeld EJ, Skalnik DG, Lievens PM, Orkin SH. Human CCAAT displacement protein is homologous to the Drosophila homeoprotein, cut. Nat. Genet. 1992; 1:50–55. [PubMed: 1301999]

Nguyen L, Besson A, Heng JI, Schuurmans C, Teboul L, Parras C, Philpott A, Roberts JM, Guillemot F. p27kip1 independently promotes neuronal differentiation and migration in the cerebral cortex. Genes Dev. 2006; 20:1511–1524. [PubMed: 16705040]

Nieto M, Monuki ES, Tang H, Imitola J, Haubst N, Khoury SJ, Cunningham J, Gotz M, Walsh CA. Expression of Cux-1 and Cux-2 in the subventricular zone and upper layers II-IV of the cerebral cortex. J. Comp. Neurol. 2004; 479:168–180. [PubMed: 15452856]

Novitch BG, Chen AI, Jessell TM. Coordinate regulation of motor neuron subtype identity and pan-neuronal properties by the bHLH repressor Olig2. Neuron. 2001; 31:773–789. [PubMed: 11567616]

Ohnuma S, Hopper S, Wang KC, Philpott A, Harris WA. Co-ordinating retinal histogenesis: early cell cycle exit enhances early cell fate determination in the Xenopus retina. Development. 2002; 129:2435–2446. [PubMed: 11973275]

Poh A, Karunaratne A, Kolle G, Huang N, Smith E, Starkey J, Wen D, Wilson I, Yamada T, Hargrave M. Patterning of the vertebrate ventral spinal cord. Int. J. Dev. Biol. 2002; 46:597–608. [PubMed: 12141448]

Quaggin SE, Heuvel GB, Golden K, Bodmer R, Igarashi P. Primary structure, neural-specific expression, and chromosomal localization of Cux-2, a second murine homeobox gene related to Drosophila cut. J. Biol. Chem. 1996; 271:22624–22634. [PubMed: 8798433]

Quinn JC, Molinek M, Martynoga BS, Zaki PA, Faedo A, Bulfone A, Hevner RF, West JD, Price DJ. Pax6 controls cerebral cortical cell number by regulating exit from the cell cycle and specifies cortical cell identity by a cell autonomous mechanism. Dev. Biol. 2007; 302:50–65. [PubMed: 16979618]

Raff MC, Durand B, Gao FB. Cell number control and timing in animal development: the oligodendrocyte cell lineage. Int. J. Dev. Biol. 1998; 42:263–267. [PubMed: 9654007]

Rao M, Sockanathan S. Transmembrane protein GDE2 induces motor neuron differentiation in vivo. Science. 2005; 309:2212–2215. [PubMed: 16195461]

Sechrist J, Bronner-Fraser M. Birth and differentiation of reticular neurons in the chick hindbrain: Ontogeny of the first neuronal population. Neuron. 1991; 7:947–963. [PubMed: 1764246]

Shen Q, Wang Y, Dimos JT, Fasano CA, Phoenix TN, Lemischka IR, Ivanova NB, Stifani S, Morrisey EE, Temple S. The timing of cortical neurogenesis is encoded within lineages of individual progenitor cells. Nat. Neurosci. 2006; 9:743–751. [PubMed: 16680166]

Sinclair AM, Lee JA, Goldstein A, Xing D, Liu S, Ju R, Tucker PW, Neufeld EJ, Scheuermann RH. Lymphoid apoptosis and myeloid hyperplasia in CCAAT displacement protein mutant mice. Blood. 2001; 98:3658–3667. [PubMed: 11739170]

Tavares AT, Tsukui T, Izpisua Belmonte JC. Evidence that members of the Cut/Cux/CDP family may be involved in AER positioning and polarizing activity during chick limb development. Development. 2000; 127:5133–5144. [PubMed: 11060239]

Temple S. The development of neural stem cells. Nature. 2001; 414:112–117. [PubMed: 11689956]

Tsuchida T, Ensini M, Morton SB, Baldassare M, Edlund T, Jessell TM, Pfaff SL. Topographic organization of embryonic motor neurons defined by expression of *LIM* homeobox genes. Cell. 1994; 79:957–970. [PubMed: 7528105]

Valarche I, Tissier-Seta JP, Hirsch MR, Martinez S, Goridis C, Brunet JF. The mouse homeodomain protein Phox2 regulates Ncam promoter activity in concert with Cux/CDP and is a putative determinant of neurotransmitter phenotype. Development. 1993; 119:881–896. [PubMed: 7910552]

Wilcock AC, Swedlow JR, Storey KG. Mitotic spindle orientation distinguishes stem cell and terminal modes of neuron production in the early spinal cord. Development. 2007; 134:1943–1954. [PubMed: 17470968]

Yang X, Tomita T, Wines-Samuelson M, Beglopoulos V, Tansey MG, Kopan R, Shen J. Notch1 signaling influences v2 interneuron and motor neuron development in the spinal cord. Dev. Neurosci. 2006; 28:102–117. [PubMed: 16508308]

Zambrowicz BP, Friedrich GA, Buxton EC, Lilleberg SL, Person C, Sands AT. Disruption and sequence identification of 2,000 genes in mouse embryonic stem cells. Nature. 1998; 392:608–611. [PubMed: 9560157]

Zhuang B, Sockanathan S. Dorsal-ventral patterning: a view from the top. Curr. Opin. Neurobiol. 2006; 16:20–24. [PubMed: 16337785]

Zimmer C, Tiveron MC, Bodmer R, Cremer H. Dynamics of Cux2 expression suggests that an early pool of SVZ precursors is fated to become upper cortical layer neurons. Cereb. Cortex. 2004; 14:1408–1420. [PubMed: 15238450]

Zimmerman L, Parr B, Lendahl U, Cunningham M, McKay R, Gavin B, Mann J, Vassileva G, McMahon A. Independent regulatory elements in the nestin gene direct transgene expression to neural stem cells or muscle precursors. Neuron. 1994; 12:11–24. [PubMed: 8292356]

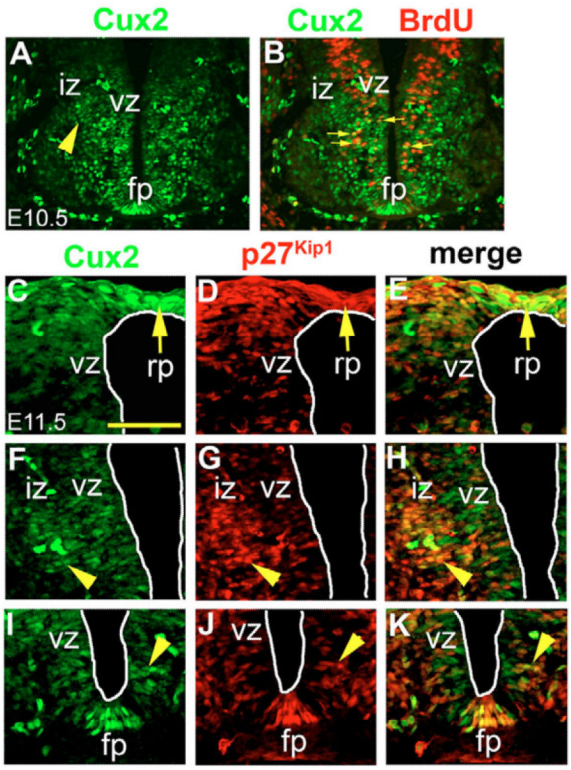

Fig. 1. Cux2 protein localizations

(**A**) In E10.5 ventral spinal cords Cux2 (green) immunostaining is localized to the vz and iz (arrowhead). (**B**) Cux2 is observed in BrdU-labeled (red) proliferating spinal cord progenitors at E10.5 (arrows). (**C–K**) Immunostaining of E11.5 spinal cords demonstrating overlapping activity of Cux2 (green) and $P27^{Kip1}$ (red) in the rp, vz and a 2–4-cell-layer-thick region outlining the iz (arrowhead) as well as the fp. Scale bar: 500 μm in C.

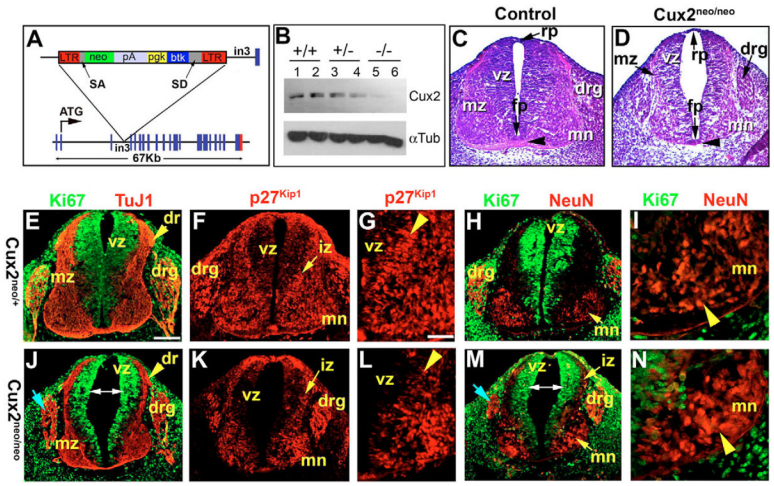

Fig. 2. Aberrant neuronal differentiation in *Cux2* mutants

(**A**) Schematic of gene trap insertion mutation in intron 3 (in3) of murine *Cux2*/*Cutl2* gene containing a promoterless neomycin (neo) selectable cassette splice acceptor (SA) and donor (SD) sites, and a long terminal repeat (LTR). (**B**) Western blot of two individual $Cux2^{+/+}$ (+/+), $Cux2^{neo/+}$ (+/−) and $Cux2^{neo/neo}$ (−/−) E12.5 embryo lysates. Cux2 protein migrated near 110 kDa. Loading control westerns for the embryo lysates showed anti-alpha Tubulin levels migrate near 50 kDa. (**C**,**D**) Hematoxylin and Eosin staining of the neural tubes of E11.5 wild-type control (C) and $Cux2^{neo/neo}$ mutant (D) embryos, which exhibit hypoplastic neural tubes and reductions in the mz, drg and ventral commissure (arrowhead). (E,J) Ki67 (green) and TuJ1 (red) staining in $Cux2^{neo/+}$ (**E**) and $Cux2^{neo/neo}$ (J) E11.5 spinal cords. (F–L) $P27^{Kip1}$ staining in $Cux2^{neo/+}$ (**F**,**G**) and $Cux2^{neo/neo}$ mutants (K,L) demonstrating reduced $p27^{Kip1}$ expression levels in the iz at E11.5. (G,L) High magnification of F,K, respectively, detailing $p27^{Kip1}$ activity in the iz (arrowhead). (J,M) Enlarged lumen (double-ended arrows) and hypoplastic drg (blue arrows). (**H–N**) Ki67 (green) and NeuN (red) expression in control $Cux2^{neo/+}$ (H,I) and $Cux2^{neo/neo}$ mutant (M,N) spinal cords. (I,N) High magnification of motoneuron domains of E11.5 $Cux2^{neo/+}$ and $Cux2^{neo/neo}$ spinal cords showing NeuN expression (red) in post-mitotic motoneurons (arrowhead). Scale bars: 250 μm in E; 500 μm in G.

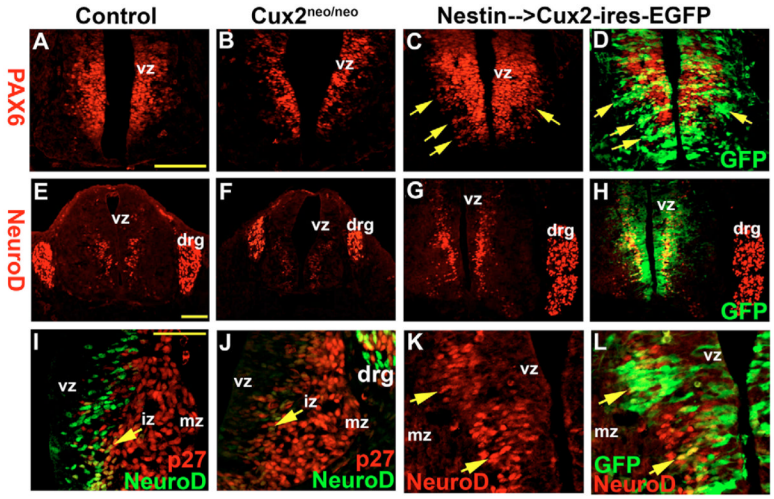

Fig. 3. Cux2 regulates neural progenitors and neuroblasts

(**A–D**) Pax6 expression in spinal cords of E11.5 wild-type (A), *Cux2*$^{neo/neo}$ (B) and *Nestin-Cux2-ires-EGFP* (C,D) embryos. (D) GFP (green) overlay on anti-Pax6 immmunohistochemistry (red) revealed a mediolateral expansion of Pax6-labeled vz cells following *Cux2* overexpression (arrows). (**E–H**) Neurod immunostaining of neuroblasts exiting the vz and also cells in the drg in E11.5 control (E), *Cux2*$^{neo/neo}$ (F) and *Nestin-Cux2-ires-EGFP* (G,H) spinal cords. (**I**,**J**) Anti-Neurod1 (green) labeling of neuroblasts in the iz (arrow) adjacent to anti-p27^{Kip1} (red) immunohistochemistry in E10.5 ventral spinal cords of control and *Cux2*$^{neo/neo}$embryos. (**K**,**L**) Enhanced Neurod1 (red) activity (arrows) in an E10.5 *Cux2* transgenic embryo overexpressing *Cux2-ires-EGFP* (green). Scale bars: 250 μm in A,E; 500 μm in I.

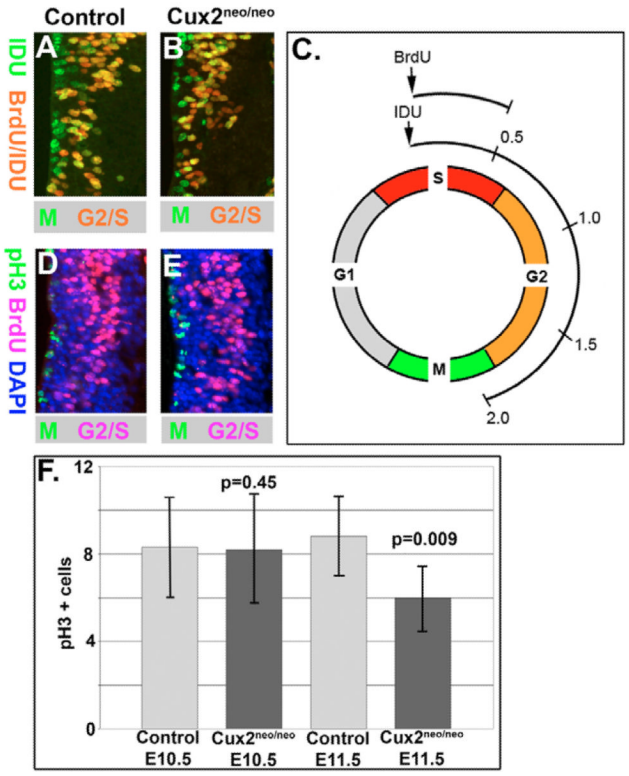

Fig. 4. Reduced cell cycle progression in *Cux2* mutants

(**A**,**B**) Detection of M phase by IDU (green), S phase by BrdU (red) and G2/S phase by IDU/BrdU (yellow/orange) labeling in E10.5 forelimb bud level neural tubes of control *Cux2*$^{neo/+}$ (A) and *Cux2*$^{neo/neo}$ mutant (B) littermates. (**C**) Schematic of IDU and BrdU pulsing regime of E10.5 pregnant dams from *Cux2*$^{+/-}$ intercrosses. (**D**,**E**) G2/S- and M-phase labeling by BrdU (fuchsia) and pH3 (green) immunohistochemistry, respectively, in neural tubes of E10.5 control (D) and *Cux2*$^{neo/neo}$ mutants. (**F**) Bar chart summarizing pH3 counts in forelimb level neural tubes at E10.5 and 11.5. *Cux2*$^{neo/neo}$ mutants displayed normal levels of pH3 staining at E10.5, but showed significant decreases in pH3 counts at E11.5 (P=0.009).

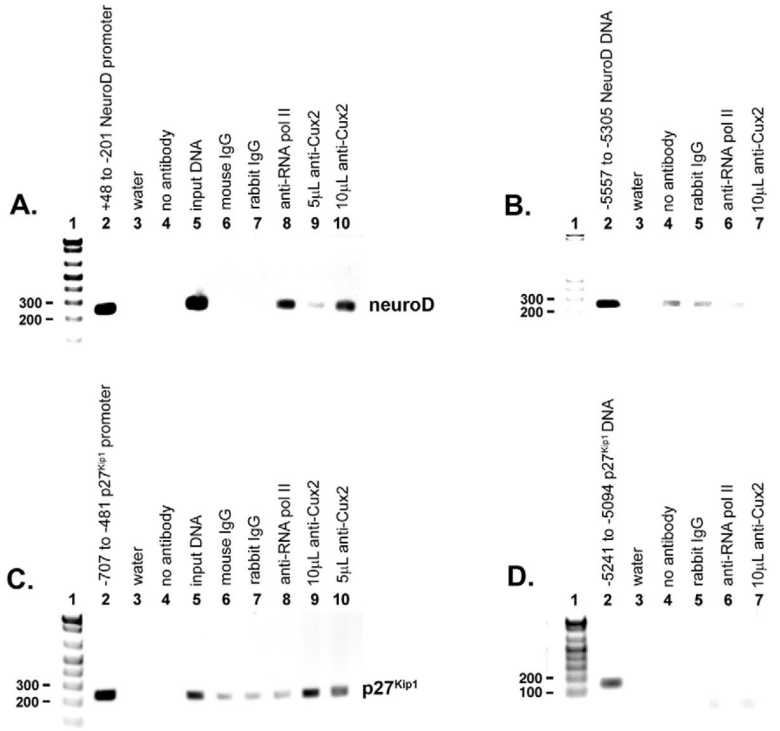

Fig. 5. *Neurod1* and *p27^{Kip1}* are direct Cux2 targets in the embryonic nervous system

Complexes isolated from E12.5 mouse brains were immunoprecipitated with either anti-Cux2 or anti-RNA polymerase II antibodies followed by reverse cross-linking of protein and DNA, and PCR amplification of a 248 bp fragment of the *Neurod1* promoter spanning +48 to −201 (A), or a 227 bp fragment of the *p27^{Kip1}* promoter spanning −707 to −481 (C), relative to the transcription start sites. (**A**) Inverse image of ethidium-stained agarose gel showing PCR amplification of a 248 bp *Neurod1* product from genomic DNA (lane 2), input DNA (lane 5), following ChIP with antibody directed against RNA polymerase II (lane 8), indicating that the *Neurod1* gene is transcriptionally active, and following ChIP with 5 μl (lane 9) or 10 μl (lane 10) of anti-Cux2 antibodies, indicating that Cux2 interacts with the *Neurod1* promoter in vivo. (**B**) To control for non-specific chromatin immunoprecipitation, a 250 bp product from −5557 to −5308 relative to the *Neurod1* transcription start site was amplified from input DNA (lane 2), following ChIP with an anti-RNA polymerase II antibody (lane 6), and following ChIP with 10 μl (lane 7) of anti-Cux2 antibodies. (**C**) PCR amplification of a 227 bp p27^{Kip1} product from genomic DNA (lane 2), input DNA (lane 5), following ChIP with anti-RNA polymerase II antibodies (lane 8), indicating that p27^{Kip1} is transcriptionally active, and following ChIP with 10 ml (lane 9) or 5 ml (lane 10) of anti-Cux2 antibodies, indicating that Cux-2 interacts with the p27^{Kip1} promoter in vivo. (**D**) To control for non-specific chromatin immunoprecipitation, a 148 bp product from −5241 to −5094 relative to the *p27^{Kip1}* transcription start site was amplified from input DNA (lane 2), following ChIP with anti-RNA polymerase II antibodies (lane 6), and following ChIP with 10 μl (lane 7) of anti-Cux2 antibodies. In both A and C, controls were water (lane 3), no antibody (lane 4), normal mouse IgG (lane 6) and normal rabbit IgG (lane 7). In both B and D, controls were water (lane 3), no antibody (lane 4) and normal rabbit IgG (lane 5).

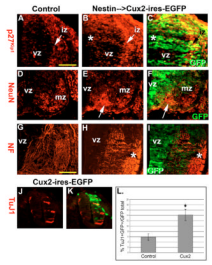

Fig. 6. Cux2 overexpression

(**A–C**) P27^{Kip1} levels (red) in E11.5 wild-type (A) and Nestin-enhancer-driven *Cux2-ires-EGFP* (green) transgenic (B–C) spinal cords in which Cux2 enhances p27^{Kip1} in the vz and iz in a cell-autonomous manner (*). (**D–F**) NeuN immunohistochemistry on E11.5 control (D) and *Cux2* transgenic (E,F) ventral spinal cords revealed that Cux2 increases NeuN-labeled post-mitotic neurons emerging from the vz (arrow). (**G–I**) Neurofilament immunohistochemistry labels axons growing towards the ventral midline in control embryos; however, in *Cux2-ires-EGFP* transgenic embryos, Cux2 overexpression induced ectopic disorganized and misdirected axons throughout the mz (*). (**J**,**K**) TuJ1 staining of HH stage 14–15 chick embryos electroporated with a murine *Cux2-ires-EGFP* vector. (**L**) Quantification of TuJ1+ and GFP+ double-positive cells following control vector or *Cux2* overexpression. **P*=0.05 by Student's *t*-test. Scale bars: 250 μm in A; 300 μm in G.

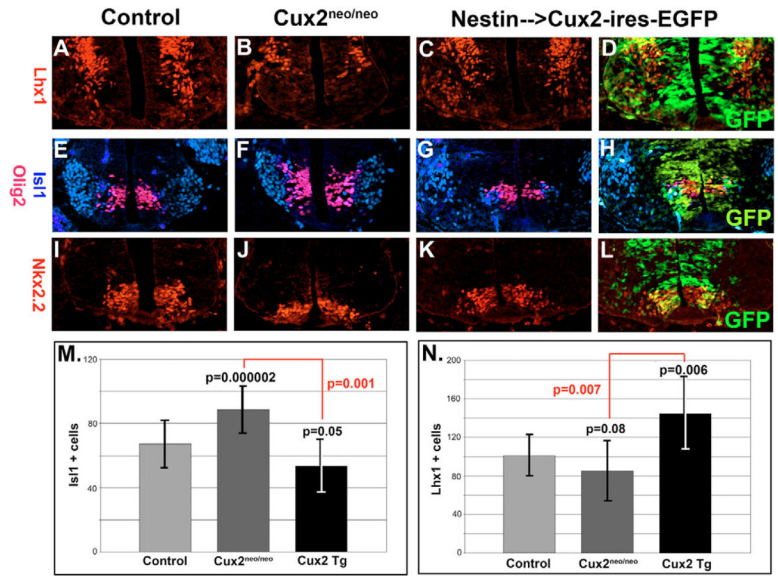

Fig. 7. Dorsoventral patterning of the spinal cord

(**A–D**) Lhx1 (red) immunostaining of interneurons in the ventral spinal cords of E10.5 control (A), *Cux2*$^{neo/neo}$ mutants (B) and *Nestin*-enhancer-driven *Cux2-ires-EGFP* transgenic (C,D) embryos. (**E–H**) Isl1 (blue) and Olig2 (red) co-labeling of control (E), *Cux2*$^{neo/neo}$ mutant (F) and *Cux2* transgenic embryos (G,H). Olig2 labels ventral motoneuron progenitors and Isl1 identifies post-mitotic motoneurons and v3 interneurons. (**I**,**J**) Nkx2.2 labeling of the ventral most progenitor domain in spinal cords from E10.5 control (I), *Cux2*$^{neo/neo}$ mutant (J) and *Cux2* transgenic (**K**,**L**) embryos. (**M**) Quantification of *Cux2* gain- and loss-of-function on Isl1-positive motoneuron formation at E10.5. *Cux2*$^{neo/neo}$ mutants (n=11) displayed a 32% increase (P=0.000003) in Isl1-positive motoneurons relative to controls (n=8), whereas *Cux2* transgenic neural tubes showed a 20% decrease (n=4, P=0.053). A 61% increase in Isl1 numbers are observed when *Cux2*$^{neo/neo}$ mutants arecompared with transgenic embryos (P=0.001). (**N**) Quantification of *Cux2* gain- and loss-of-function on the formation of Lhx1-positve ventral interneurons at E10.5. *Cux2*$^{neo/neo}$ mutants displayed a 16% decrease (n=8, P=0.08) in Lhx1-positive cells relative to controls (n=4), while *Cux2* transgenic neural tubes showed a 43% increase (n=4, P=0.006). A 70% decrease in Lhx1 numbers are observed when *Cux2*$^{neo/neo}$ mutants are compared with transgenic embryos (P=0.0007). Data are summarized in Table S2 in the supplementary material.

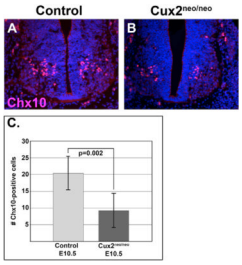

Fig. 8. Cux2 and V2 interneuron formation

(**A**,**B**) Expression of homeodomain transcription factor Chx10 in V2 interneurons in the spinal cords of E10.5 wild-type (A) and *Cux2*$^{neo/neo}$ (B) embryos.(**C**) *Cux2*$^{neo/neo}$ mutants (*n*=8; 9.25±5.09) displayed a 45% decrease (*P*=0.002) in Chx10-positive V2 interneurons relative to controls (*n*=5; 20.40±5.03). The average values of Chx10-positive cells were plotted with error bars reflecting the standard deviation from the mean.

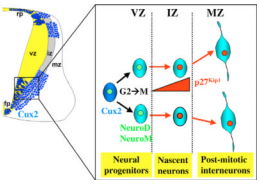

Fig. 9. Model for the dual role of *Cux2* in spinal cord neurogenesis

Cux2 activity stimulates the cell-cycle progression of neural progenitors in the spinal cord vz. In so doing, Cux2 initiates a neuroblast gene expression program that includes the bHLH factor Neurod, and subsequently directs these populations to exit the cell cycle by inducing $p27^{Kip1}$ in the iz. Cux2 activity in neural progenitors also biases their fate to mature interneurons (IN) in the mz, thereby acting as a cell-fate selector in nascent neurons.

Table 1

Cux2$^{neo/neo}$ mutants display reduced progression through mitosis in the developing spinal cords at E10.5

	Scells (IDU+BrdU)	Lcells (IDU only)	Ts (S-phase length)
Control E10.5 (*n*=14)*	33.3±7.2†	20.6±5.0	2.4±0.5
Cux2$^{neo/neo}$ E10.5 (*n*=8)	43.1±7.7	16.4±2.7	3.9±0.7
P value (*t*-test)‡	0.005	0.01	0.0001

Embryos were pulsed with IDU for a total of 2 hours and BrdU for 0.5 hours prior to harvesting. The fraction of cells within S phase of the cell cycle (Scells) is represented by the total of IDU and BrdU double-labeled nuclei (yellow signal in Fig. 5), whereas the fraction of cells in G2/M (Lcells) was obtained from counting the nuclei labeled with IDU alone (green in Fig. 5). The S-phase length was determined using the following formula: Scells/Lcells×1.5 hours.

*For control littermates, a total of 14 sections from four different embryos were used. For *Cux2*$^{neo/neo}$ embryos, a total of eight sections from three different mutants were used. IDU and BrdU positive nuclei were counted from the unilateral halves of ventral neural tubes at E10.5.

†Figures are represented as average values±s.d.

‡P values were determined using a one-tailed Student's *t*-test with two samples, unequal variance.